Hindawi
Shock and Vibration
Volume 2019, Article ID 1746563, 9 pages
https://doi.org/10.1155/2019/1746563

Research Article

Eliminating the Fluid-Induced Vibration and Improving the Stability of the Rotor/Seal System Using the Inerter-Based Dynamic Vibration Absorber

Qi Xu,[1] **Yuanqing Luo**,[1] **Hongliang Yao**,[2] **Lichao Zhao**,[3] **and Bangchun Wen**[2]

[1]*School of Mechanical Engineering, Shenyang University of Technology, Shenyang 110870, China*
[2]*School of Mechanical Engineering and Automation, Northeastern University, Shenyang 110819, China*
[3]*Installation Accessories Co. Ltd., Shenyang Blower Group Co. Ltd., Shenyang 110869, China*

Correspondence should be addressed to Hongliang Yao; hlyao@mail.neu.edu.cn

Received 5 June 2019; Accepted 17 August 2019; Published 2 September 2019

Academic Editor: Marco Lepidi

A theoretical research on eliminating the instability vibration and improving the stability of the rotor/seal system using the inerter-based dynamic vibration absorber (IDVA) is presented in this paper. The modified Jeffcott rotor and Muszynska nonlinear seal force models are employed. The proposed IDVA is the damping element of the traditional dynamic vibration absorber (DVA) replaced by one of the six configurations of the inerter. The instability threshold speed of the system is obtained by applying the Routh–Hurwitz stability criterion. The quantum particle swarm optimization (QPSO) method is utilized to optimize the parameters of the IDVA. The numerical method is applied to investigate the nonlinear dynamic responses and stability. The results show that the IDVA can effectively improve the stability and reduce the instability vibration of the rotor/seal system. Furthermore, the performance of the IDVA is more effective than that of the traditional DVA.

1. Introduction

The nonlinear seal force between the rotor and seal is prone to the instability vibration in the rotating machine. The instability vibration is one kind of the self-excited vibrations and adversely causes the amplitude to increase dramatically. Hence, the instability vibration must be controlled.

Great efforts for the instability vibration control had been made by Bently and Muszynska [1]. The nonlinear behavior and stability had been analysed via the Bently/Muszynska (B/M) nonlinear seal force model. The expression of the instability threshold was defined, and the "cross stiffness" component was the main reason for the instability. The fluid circumferential average velocity ratio is considered a key parameter for the instability vibration control. It can be realized using the various seals to disrupt the fluid flow [2–4]. The antiswirl flow in the seal was a typical method to eliminate the instability [5]. It was widely used in engineering. Zhang et al. [6] computed the dynamic and flow characteristics of the honeycomb seal and corresponding labyrinth seal in the rotor, and the results showed that the instability vibration could be reduced due to the additional aerodynamic force generated by the seal. Then, they presented two types of the labyrinth seals in the rotor system: the straight-through and corresponding interlaced labyrinth seal. The dynamic and flow characteristics of the rotor/seal system were analysed by the numerical method, and it showed that the straight-through labyrinth seal could reduce the rotor instability vibration [7]. Jia et al. [8] investigated the dynamic leakage rate of the rotor-labyrinth seal system with the variable rotating speed. The similar conclusion that the labyrinth seal could improve the rotor stability was obtained. Zhang et al. [9]

studied dynamic characteristics of the rotor/bearing/labyrinth-seal system. The research indicated that the shorter seal length could improve the stability of the rotor system, but the sealing effect was decreased.

Recently, the DVA has begun to attract attention to eliminate the rotor vibration. Hu and He [10] designed a rotor DVA to online control the rotor critical speed vibration and discussed the effect of the installation position on the suppression performance. Heidari and Monjezi [11] investigated the vibration control of the unbalanced rotor using the virtual passive DVA with the optimal parameters. The permanent magnet DVAs with the negative and tunable stiffness were presented to reduce the rotor unbalance vibration by Yao et al. [12, 13]. Besides, the nonlinear energy sink (NES, a kind of the nonlinear stiffness DVA) and centrifugal pendulum vibration absorber (CPVA, a kind of the torsion DVA) have been applied for the antiresonance and torsional vibration suppression of the rotor, respectively. For example, Taghipour et al. [14] studied the antiresonance for the nonlinear bearing of the rotor with the DVA and NES. Tehrani and Dardel [15] investigated the DVA and NES to prevent the contact between the rotor and stator. The NES was also employed for the vibration control of the unbalanced hollow rotor [16] and continuous rotor-blisk-journal bearing system [17]. Shi et al. [18] and Nishimura [19] et al. described the torsional vibration reduction in the rotor using the CPVA.

Now that the inerter, which is proposed for the vibration control of the vehicle suspension [20], has already been applied in the DVA, called the IDVA. Hu and Chen [21] investigated the parameter optimization to improve the performance of the IDVA. The extended fixed-point theory was used for the parameter optimization of the IDVA [22, 23]. Lazarek et al. [24] designed a tuned mass damper with the variable inerter. The IDVA has been utilized to the vibration control of the cable [25, 26], the offshore wind turbine [27], tall building [28], and so on.

The traditional DVA could eliminate the instability vibration in the rotor/seal system [29, 30]. The fluid-induced instability elimination of the rotor with the IDVA is proposed in this paper. First, the model of the rotor/seal system with the IDVA is established. Second, the expression of the instability threshold speed is obtained. Third, the numerical calculation is employed for the nonlinear dynamic and stability analysis. Then, the performance comparison between the IDVA and traditional DVA is discussed. Finally, some conclusions are drawn to summarize the effects of the fluid-induced vibration elimination and stability region extension on the rotor/seal system by the IDVA.

2. Model of Rotor/Seal System with IDVA

Figure 1shows the model of the rotor/seal system with the IDVA. The instability vibration usually happens in the turbomachinery, such as the centrifugal compressor. Normally, the running speed of the kind of the rotor system is between the first- and second-order critical speeds. Therefore, the modified Jeffcott rotor model and B/M nonlinear seal force model are employed for the rotor/seal system model [1, 29]. The rotor model is employed for considering the first-order vibration shape. The nonlinear dynamic behaviors and stability of the real rotor/seal system can be described by the models. The IDVA is added in the rotor in the perpendicular directions by the rolling bearing in order to avoid rotation with the rotor [10]. The DVA and IDVA are depicted in Figure 2. The damping element of the DVA is replaced by one of the six configurations of the inerter: c_1, c_2, c_3, c_4, c_5, and c_6 [21]. Taking c_3 as an example in the main part of this paper, the equations of motion for the rotor/seal system with the IDVA are as follows:

$$\begin{cases} m\ddot{x} + d\dot{x} + kx + f_{x\mathrm{Seal}} + k_{\mathrm{a}}(x - x_{\mathrm{a}}) + f_{x\mathrm{IDVA}} \\ \quad = m_{\mathrm{e}}\omega^2 r\cos\omega t, \\ m\ddot{y} + d\dot{y} + ky + f_{y\mathrm{Seal}} + k_{\mathrm{a}}(y - y_{\mathrm{a}}) + f_{y\mathrm{IDVA}} \\ \quad = m_{\mathrm{e}}\omega^2 r\sin\omega t, \\ m_{\mathrm{a}}\ddot{x}_{\mathrm{a}} + k_{\mathrm{a}}(x_{\mathrm{a}} - x) - f_{x\mathrm{IDVA}} = 0, \\ m_{\mathrm{a}}\ddot{y}_{\mathrm{a}} + k_{\mathrm{a}}(y_{\mathrm{a}} - y) - f_{y\mathrm{IDVA}} = 0, \end{cases} \tag{1}$$

where m, d, and k are the rotor generalized mass, lateral external damping, and lateral isotropic stiffness, respectively. m_{e} and r denote, respectively, the eccentric mass and eccentricity. ω is the rotating speed. m_{a} and k_{a} denote, respectively, the mass and stiffness coefficients of the IDVA. x, y, x_{a}, and y_{a} are the horizontal and vertical displacement generalized coordinates of the rotor and IDVA, respectively. $f_{x\mathrm{Seal}}$ and $f_{y\mathrm{Seal}}$ are the components of the nonlinear seal force in the x and y directions, respectively. The expressions are

$$\begin{cases} f_{x\mathrm{Seal}} = m_{\mathrm{f}}\ddot{x} + d_{\mathrm{f}}\dot{x} + 2m_{\mathrm{f}}\omega\lambda\dot{y} + \left(k_{\mathrm{f}} - m_{\mathrm{f}}\omega^2\lambda^2\right)x + \omega d_{\mathrm{f}}\lambda y, \\ f_{y\mathrm{Seal}} = m_{\mathrm{f}}\ddot{y} - 2m_{\mathrm{f}}\omega\lambda\dot{x} + d_{\mathrm{f}}\dot{y} - \omega d_{\mathrm{f}}\lambda x + \left(k_{\mathrm{f}} - m_{\mathrm{f}}\omega^2\lambda^2\right)y, \end{cases} \tag{2}$$

where m_{f}, d_{f}, and k_{f} denote, respectively, the seal fluid inertia, seal fluid film radial damping, and seal fluid stiffness coefficients. λ is the seal fluid circumferential average velocity ratio. The expressions of the nonlinear terms are

$$\begin{aligned} d_{\mathrm{f}} &= d_0\left(1 - z^2\right)^{-n}, \\ k_{\mathrm{f}} &= k_0\left(1 - z^2\right)^{-n}, \\ \lambda &= \lambda_0(1 - z)^b, \\ z &= \frac{\sqrt{x^2 + y^2}}{r_{\mathrm{f}}}, \end{aligned} \tag{3}$$

where d_0, k_0, λ_0, n, and b are the parameters of the nonlinear seal force. These parameters of the nonlinear force are described in detail by Bently and Muszynska [1, 31]. r_{f} is the radial clearance of the seal.

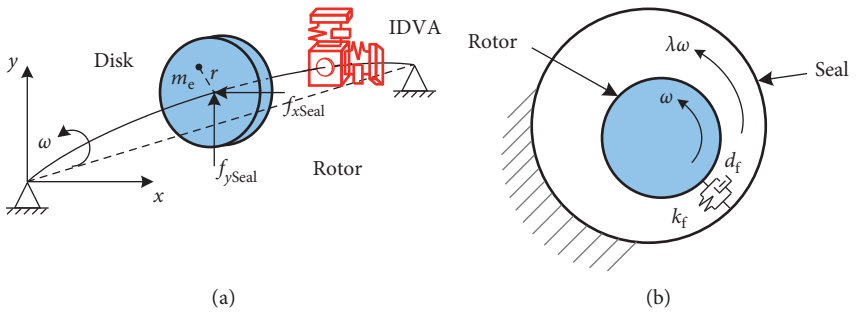

Figure 1: The model of the rotor/seal system with the IDVA.

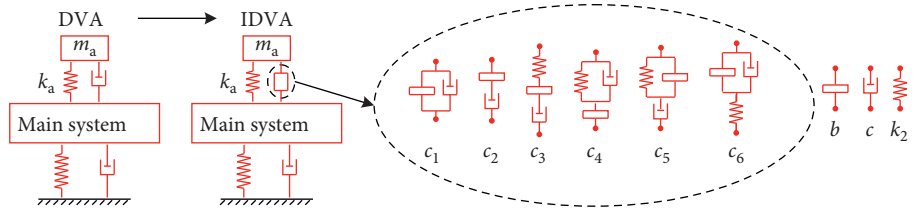

Figure 2: The model of the DVA and IDVA.

$f_{x\mathrm{IDVA}}$ and $f_{y\mathrm{IDVA}}$ denote, respectively, the force components of the IDVA that acted on the rotor in the x and y directions. The expressions are as follows:

$$\begin{cases} f_{x\mathrm{IDVA}} = c(\dot{x} - \dot{x}_c) = k_2(x_k - x_a) = b(\ddot{x}_c - \ddot{x}_k), \\ f_{y\mathrm{IDVA}} = c(\dot{y} - \dot{y}_c) = k_2(y_k - y_a) = b(\ddot{y}_c - \ddot{y}_k), \end{cases} \tag{4}$$

where b, c, and k_2 are the inertance, damping, and stiffness coefficients of the configuration of the inerter. x_c and y_c denote, respectively, the generalized displacements between the inertance and damping element in the x and y directions. x_k and y_k denote, respectively, the generalized displacements between the inertance and stiffness element in the x and y directions.

To define the dimensionless parameters:

$$\begin{aligned} \varepsilon_e &= \frac{m_e}{m}, \\ \varepsilon_f &= \frac{m_f}{m}, \\ \varepsilon_a &= \frac{m_a}{m}, \\ \varepsilon_b &= \frac{b}{m_a}, \\ \zeta &= \frac{d}{2\sqrt{km}}, \\ \zeta_a &= \frac{c}{2\sqrt{k_a m_a}}. \end{aligned} \tag{5}$$

The dimensionless transform is as following:

$$\begin{aligned} &\begin{cases} X = \dfrac{x}{r_f}, \\ Y = \dfrac{y}{r_f}, \end{cases} \\ &\begin{cases} X_a = \dfrac{x_a}{r_f}, \\ Y_a = \dfrac{y_a}{r_f}, \end{cases} \\ &\begin{cases} X_c = \dfrac{x_c}{r_f}, \\ Y_c = \dfrac{y_c}{r_f}, \end{cases} \\ &\begin{cases} X_k = \dfrac{x_k}{r_f}, \\ Y_k = \dfrac{y_k}{r_f}, \end{cases} \\ &\tau = \omega t, \end{aligned} \tag{6}$$

and define the generalized coordinates (Taking the x coordinate as an example):

$$\begin{aligned} \dot{x} &= \frac{d}{dt}x = \omega\frac{d}{d\tau}x = \omega x', \\ \ddot{x} &= \frac{d^2}{dt^2}x = \omega^2\frac{d^2}{d\tau^2}x = \omega^2 x''. \end{aligned} \tag{7}$$

Conveniently, the dimensionless generalized coordinates are still expressed as x, y, x_a, y_a, x_c, y_c, x_k, and y_k, respectively. The original equations become the dimensionless equations:

$$\begin{cases} x'' + 2\zeta\overline{\omega}_r x' + \overline{\omega}_r^2 x + \overline{f}_{x\text{Seal}} + \varepsilon_a\overline{\omega}_a^2(x - x_a) + \overline{f}_{x\text{IDVA}} \\ \quad = \varepsilon_e \cos\tau, \\ y'' + 2\zeta\overline{\omega}_r y' + \overline{\omega}_r^2 y + \overline{f}_{y\text{Seal}} + \varepsilon_a\overline{\omega}_a^2(y - y_a) + \overline{f}_{y\text{IDVA}} \\ \quad = \varepsilon_e \sin\tau, \\ x_a'' + \overline{\omega}_a^2(x_a - x) - \overline{f}_{x\text{IDVA}} = 0, \\ y_a'' + \overline{\omega}_a^2(y_a - y) - \overline{f}_{y\text{IDVA}} = 0, \end{cases} \tag{8}$$

where

$$\begin{aligned} \overline{\omega}_r &= \frac{\omega_r}{\omega}, \\ \omega_r &= \sqrt{\frac{k}{m}}, \\ \overline{\omega}_a &= \frac{\omega_a}{\omega}, \\ \omega_a &= \sqrt{\frac{k_a}{m_a}}. \end{aligned} \tag{9}$$

The dimensionless components of the nonlinear seal force:

$$\begin{cases} \overline{f}_{x\text{Seal}} = \varepsilon_f x'' + \mu_d x' + 2\varepsilon_f\lambda y' + \left(\mu_k - \varepsilon_f\lambda^2\right)x + \mu_d\lambda y, \\ \overline{f}_{y\text{Seal}} = \varepsilon_f y'' - 2\varepsilon_f\lambda x' + \mu_d y' - \mu_d\lambda x + \left(\mu_k - \varepsilon_f\lambda^2\right)y, \end{cases} \tag{10}$$

where

$$\begin{aligned} \mu_d &= \frac{d_f}{m\omega}, \\ \mu_k &= \frac{k_f}{m\omega^2}. \end{aligned} \tag{11}$$

The dimensionless force components of the IDVA acted on the rotor:

$$\begin{cases} \overline{f}_{x\text{IDVA}} = 2\zeta_a\overline{\omega}_a(\dot{x} - \dot{x}_c) = \varepsilon_b\overline{\omega}_b^2(x_k - x_a) = \varepsilon_b(\ddot{x}_c - \ddot{x}_k), \\ \overline{f}_{y\text{IDVA}} = 2\zeta_a\overline{\omega}_a(\dot{y} - \dot{y}_c) = \varepsilon_b\overline{\omega}_b^2(y_k - y_a) = \varepsilon_b(\ddot{y}_c - \ddot{y}_k), \end{cases} \tag{12}$$

where

$$\begin{aligned} \overline{\omega}_b &= \frac{\omega_b}{\omega}, \\ \omega_b &= \sqrt{\frac{k_2}{b}}. \end{aligned} \tag{13}$$

3. Stability Analysis

The unbalance force is assumed zero, the nonlinear terms and seal fluid inertia coefficient are neglected as they are minimal for the stability analysis [32]. The original dimensionless equations (8) can be rewritten:

$$\begin{cases} x'' + 2\zeta\overline{\omega}_r x' + \overline{\omega}_r^2 x + \mu_d x' + \mu_k x + \mu_d\lambda y + \varepsilon_a\overline{\omega}_a^2(x - x_a) \\ \quad + \overline{f}_{x\text{IDVA}} = 0, \\ y'' + 2\zeta\overline{\omega}_r y' + \overline{\omega}_r^2 y + \mu_d y' - \mu_d\lambda x + \mu_k y + \varepsilon_a\overline{\omega}_a^2(y - y_a) \\ \quad + \overline{f}_{y\text{IDVA}} = 0, \\ x_a'' + \overline{\omega}_a^2(x_a - x) - \overline{f}_{x\text{IDVA}} = 0, \\ y_a'' + \overline{\omega}_a^2(y_a - y) - \overline{f}_{y\text{IDVA}} = 0. \end{cases} \tag{14}$$

The characteristic equation can be obtained:

$$\begin{aligned} a_0\mu^{2q} + a_1\mu^{2q-1} + a_2\mu^{2q-2} + \cdots + a_{2q-3}\mu^3 + a_{2q-2}\mu^2 + a_{2q-1}\mu \\ + a_{2q} = 0, \end{aligned} \tag{15}$$

where μ is the eigenvalue and q is the degree of freedom of equation (14). a_0, a_1, a_2, ..., a_{2q} are the coefficients of the characteristic equation.

According to the Routh-Hurwitz stability criterion [33], the instability threshold speed ω_i of the rotor system can be obtained from the following expressions:

$$\begin{aligned} a_0, a_1, \ldots, a_{2q} > 0, \\ H_1, H_2, \ldots, H_{2q-2} > 0, \\ H_{2q-1} = 0, \end{aligned} \tag{16}$$

where H is the Hurwitz determinant, and:

$$H_{2q} = \begin{vmatrix} a_1 & a_3 & a_5 & \cdots & 0 \\ a_0 & a_2 & a_4 & \cdots & 0 \\ 0 & a_1 & a_3 & \cdots & 0 \\ 0 & a_0 & a_2 & \cdots & 0 \\ \vdots & \vdots & \vdots & \ddots & \vdots \\ 0 & 0 & 0 & \cdots & a_{2q} \end{vmatrix}. \tag{17}$$

The rotor/seal system is stable as $\omega < \omega_i$ and unstable as $\omega > \omega_i$.

4. Numerical Simulations and Discussion

The numerical calculation is employed due to the complicated nonlinear terms of equation (8) and implicit equation (16). The parameters of the rotor/seal system are obtained from reference [29] in order to compare with the previous research. The rotor $m = 1$ kg, $\zeta = 0.025$, $\omega_r = 200$ rad/s, $r_f = 10^{-3}$ m and $\varepsilon_e = 0.01$. The nonlinear seal force $\varepsilon_f = 10^{-6}$, $d_0 = 100$ Nm/s, $k_0 = 1$ N/m, $\lambda_0 = 0.48$, $n = 2$ and $b = 0.5$. Assuming that the dimensionless rotating speed $s = \omega/\omega_r$, the frequency ratio $\sigma_a = \omega_a/\omega_r$ and $\sigma_b = \omega_b/\omega_r$. The QPSO algorithm is utilized to obtain the optimal IDVA parameters. The target function is the rotor instability threshold speed ω_i. The mass ratio $\varepsilon_a = 0.01$ and ε_b is a constant. Moreover, the damping ratio ζ_a, dimensionless frequency ratio σ_a and σ_b

are the optimization parameter. Correspondingly, the parameter optimization ranges are $0 < \zeta_a < 1$, $0 < \sigma_a \leq 2$ and $0 < \sigma_b \leq 2$, respectively. The flow chart of the QPSO method is shown in Figure 3.

The optimization results are shown in Table 1. It can be seen that the maximum of the instability threshold speed is $\omega_i = 2.759$ as $\varepsilon_b = 0.03$, $\zeta_a = 0.05$, $\sigma_a = 0.98$, and $\sigma_b = 0.95$. The convergence diagram of the optimization as $\varepsilon_b = 0.03$ is in Figure 4. It shows that the optimization is convergent as the number of the iterations is greater than 15.

Therefore, the parameters of the IDVA are selected as follows: $\varepsilon_b = 0.03$, $\zeta_a = 0.05$, $\sigma_a = 0.98$, and $\sigma_b = 0.95$. The changes of the coefficients in equation (15) and Hurwitz determinants to estimate the stability are presented in Figure 5. It can be seen that $a_0, a_1, a_2, \ldots, a_{12}$ are positive (Figure 5(a)); $H_1, H_2, \ldots, H_8$ are also positive (Figure 5(b)), H_9 and H_{10} are also positive at $s \leq 2.76$, and H_{11} is equal to zero when s is between 2.755 and 2.76 (Figure 5(c)). The coefficients and Hurwitz determinants satisfy the Routh–Hurwitz stability criterion. The bifurcation diagram, amplitude-frequency response curve, frequency spectrum, orbit, and Poincaré map are used to investigate the nonlinear behavior by the Newmark time integration method [34]. The algorithm is unconditionally convergent as the values of parameters $\beta \geq 1/4$ and $\delta \geq 1/2$ [35].

The bifurcation diagram and amplitude-frequency response curve of the rotor/seal system in the x coordinate are shown in Figure 6. The blue and red solid dots and lines are the bifurcation and amplitude-frequency response curve of the rotor/seal system without and with the IDVA, respectively. It can be observed in Figure 6(a) that the vibration of the rotor/seal system is synchronous to one period at $s < 2.31$. Only one point is correspondingly shown in the bifurcation diagram for every rotating speed. Then, the vibration changes and bifurcates at $s = 2.31$. The vibration is double-periodic, multiperiodic, or quasi-periodic at $s \geq 2.31$ and can be determined by using the Poincaré map. $s = 2.31$ is the instability threshold speed of the rotor/seal system. The variances of the vibration in the rotor/seal system as adding the IDVA are as follows: the vibration of the system is synchronous to one period at $s < 2.805$; then the vibration changes and bifurcates at $s = 2.805$; the vibration is double-periodic, multiperiodic, or quasi-periodic at $s \geq 2.805$ and can be determined by using the Poincaré map; and $s = 2.805$ is the instability threshold speed of the rotor/seal system. Comparing with the rotor/seal system without the IDVA, the instability threshold speed increases by about 21.43%. The instability vibration between $s = 2.31$ and $s = 2.805$ becomes the synchronous vibration. The instability vibration is eliminated completely in this range. Simultaneously, the instability threshold speed increases by about 1.67% comparing with Table 1. The result illustrates that the instability threshold obtained by the linear equation (16) is less than that obtained by the nonlinear equation (8). Whether or not to add the IDVA, the amplitude of the system increases rapidly when the rotating speed exceeds the instability threshold speed as shown in Figure 6(b). But the instability amplitude can be reduced by the IDVA at $s \geq 2.805$. The instability vibration is eliminated partially in this range.

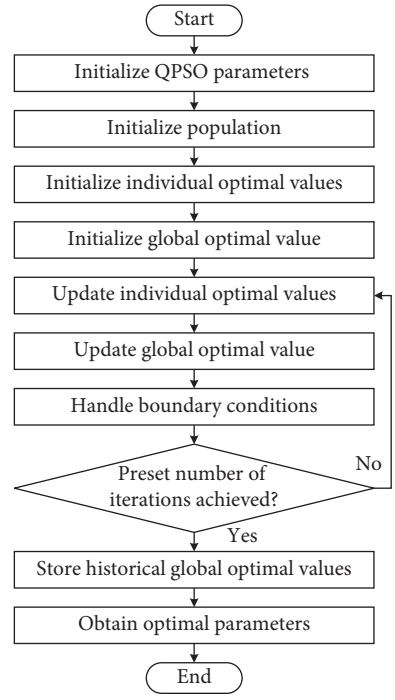

Figure 3: The flow chart of the QPSO algorithm.

Table 1: The parameters optimization results of the IDVA

ε_b	Optimized ζ_a	Optimized σ_a	Optimized σ_b	ω_i
0.01	0.05	0.98	1	2.743
0.02	0.04	0.99	0.98	2.756
0.03	**0.05**	**0.98**	**0.95**	**2.759**
0.04	0.05	0.98	0.94	2.750
0.05	0.05	0.98	0.92	2.753
0.06	0.05	0.98	0.91	2.745
0.07	0.05	0.98	0.90	2.739
0.08	0.06	0.97	0.85	2.735
0.09	0.05	0.98	0.88	2.731
0.10	0.05	0.98	0.87	2.728

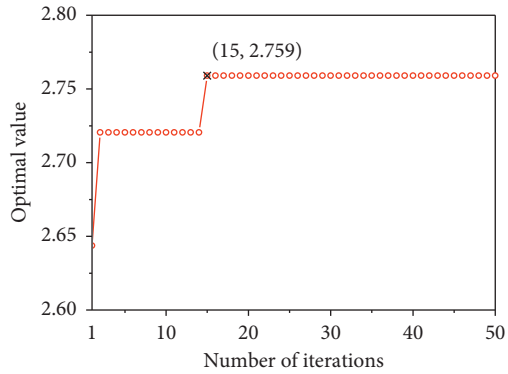

Figure 4: The optimization convergence result of the IDVA as $\varepsilon_b = 0.03$.

The speed $s = 2$, $s = 2.5$, and $s = 3$ are picked, respectively, for the dynamic behavior analysis in the range of $s < 2.31$, $2.31 < s < 2.805$, and $s > 2.805$ as shown in Figures 7–9. The blue and red solid dots and lines are the response of the

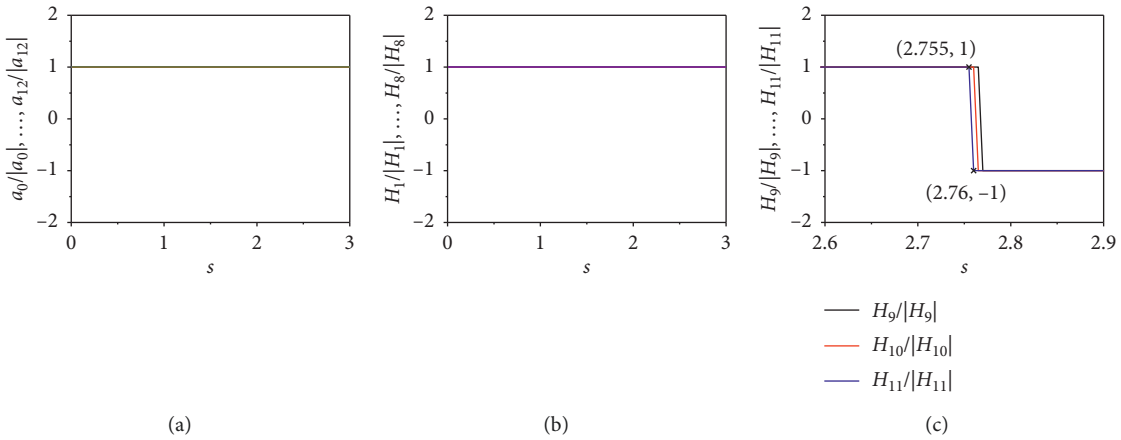

Figure 5: The coefficients of the characteristic equation and Hurwitz determinants change with the speed.

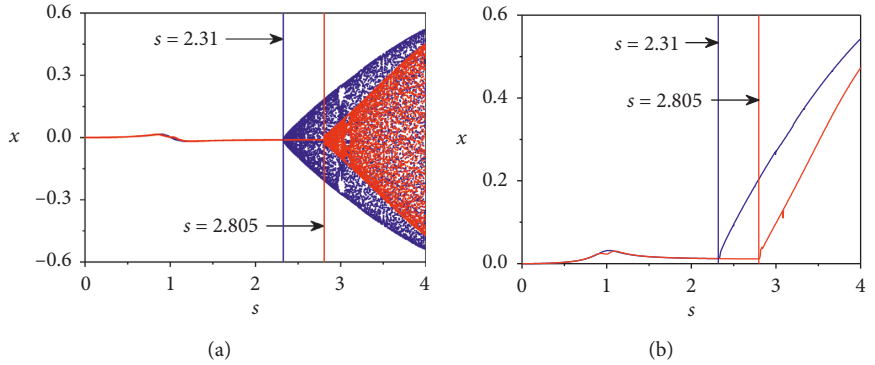

Figure 6: (a) The bifurcation diagram and (b) the amplitude-frequency response curve of the rotor/seal system in the x coordinate.

rotor/seal system without and with the IDVA, respectively. Figure 7 presents the response is synchronous to one period, and there is less change after adding the IDVA as the speed $s = 2$ is away from the resonance region. The response is five-periodic when $s = 2.5$ as shown in Figure 8. The instability vibration frequency is close to the first-order natural frequency of the rotor. The amplitude of the instability frequency is much higher than that of the rotating frequency. Then the response becomes one period, and the instability frequency disappears after adding the IDVA. As the speed continues to increase, Figure 9 represents the response is three-periodic when $s = 3$. The response becomes quasi-period, and the instability frequency is eliminated partially after adding the IDVA.

5. Comparison with the Previous Work

The traditional DVA has been applied to eliminate the instability vibration in the rotor/seal system in reference [29]. The comparison results of the instability threshold speed are shown in Table 2. It can be seen that the instability threshold speed of the rotor with the IDVA is larger than that of the rotor with the traditional DVA except the configuration of the inerter c_2. The maximum instability threshold speed is obtained from the configuration of the inerter c_3.

The comparison results of the bifurcation diagram and amplitude-frequency response curve are shown in Figure 10. The black and red solid dots and lines are the response of the rotor/seal system with the traditional DVA and IDVA, respectively. It can been seen that the instability threshold speed of the rotor with the IDVA (c_3) is larger than that of the rotor with the traditional DVA, and the instability amplitude of the rotor with the IDVA (c_3) is less than that of the rotor with the traditional DVA. The result still illustrates that the linear model appears more conservative in evaluating instability.

The comparison results of the relationship between the instability threshold speed and frequency ratio σ_a and the instability threshold speed and damping ratio ζ_a are shown in Figure 11. The black dashed line represents the instability threshold speed of the rotor. Comparing the rotor with the traditional DVA, Figure 11(a) shows that the range of increase in instability threshold speed is almost constant as the frequency ratio σ_a changes, while Figure 11(b) shows that the range of increase in instability threshold speed is decreased as the damping ratio ζ_a changes. And the maximum of the instability threshold speed increases by about 3.13%.

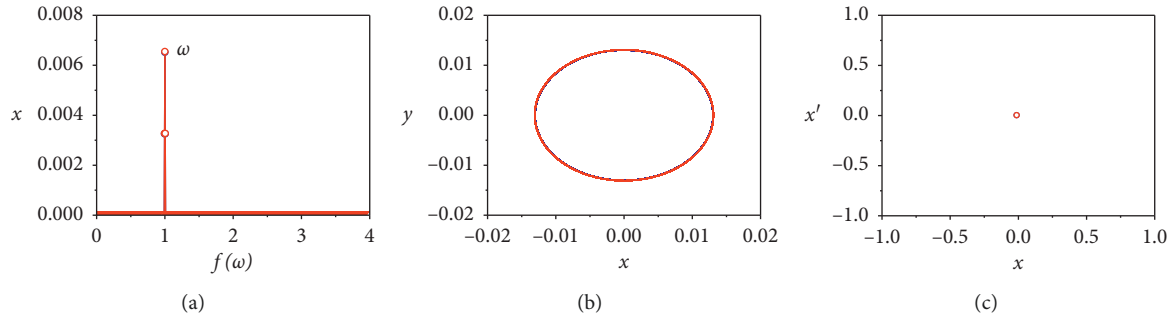

Figure 7: The response of the rotor/seal system at $s = 2$. (a) The frequency spectrum of the x coordinate. (b) The orbit of the rotor. (c) The Poincaré map of the x coordinate.

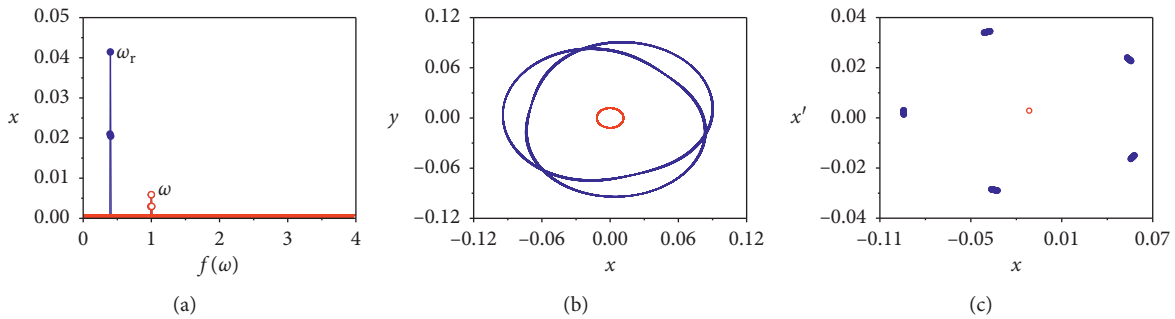

Figure 8: The response of the rotor/seal system at $s = 2.5$. (a) The frequency spectrum of the x coordinate. (b) The orbit of the rotor. (c) The Poincaré map of the x coordinate.

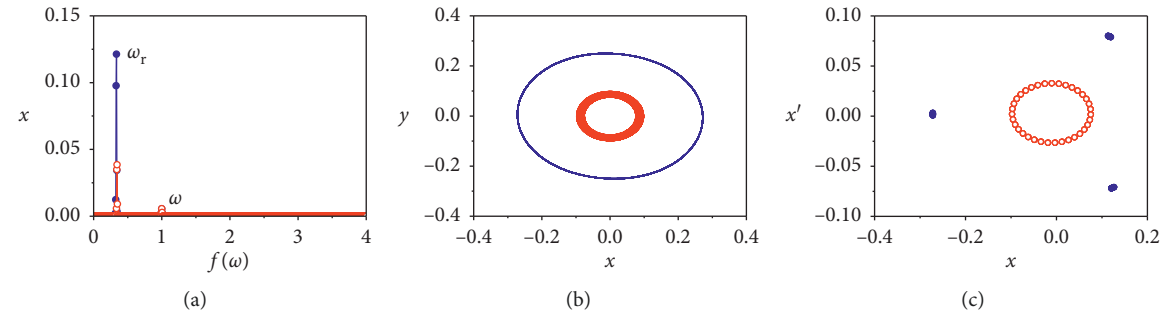

Figure 9: The response of the rotor/seal system at $s = 3$. (a) The frequency spectrum of the x coordinate. (b) The orbit of the rotor. (c) The Poincaré map of the x coordinate.

Table 2: The comparison results of the instability threshold speed.

	ε_b	Optimized ζ_a	Optimized σ_a	Optimized σ_b	ω_i	Increment
DVA	—	0.05	0.99	—	2.687	—
IDVAc_1	0.01	0.05	1.00	—	2.696	+0.33%
IDVAc_2	0.10	0.05	1.00	—	2.504	−6.81%
IDVAc_3	0.03	0.05	0.98	0.95	2.759	+2.68%
IDVAc_4	0.09	0.03	1.01	0.76	2.728	+1.53%
IDVAc_5	0.09	0.14	0.93	1.79	2.730	+1.60%
IDVAc_6	0.04	0.01	0.98	1.03	2.755	+2.53%

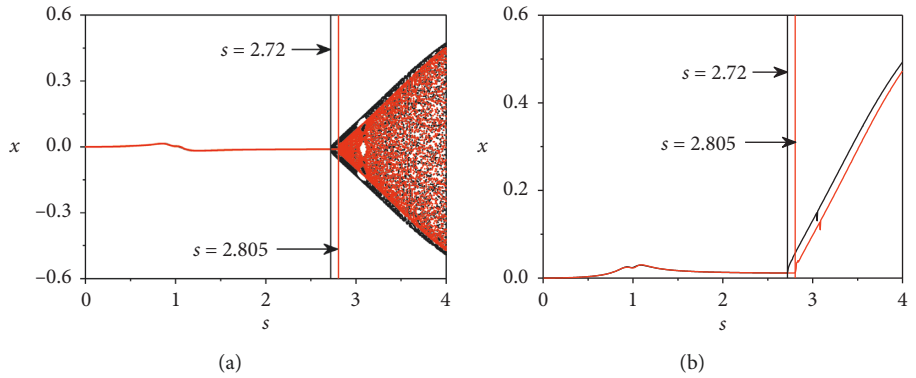

Figure 10: The comparison results of (a) the bifurcation diagram and (b) the amplitude-frequency response curve.

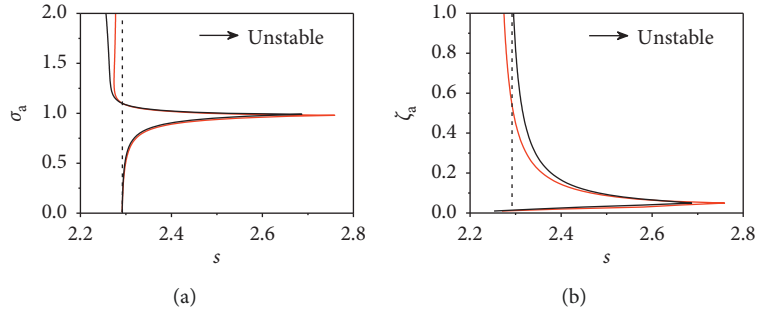

Figure 11: The comparison results of the relationship between instability threshold speed and (a) the frequency ratio σ_a and (b) the damping ratio ζ_a.

6. Conclusions

The fluid-induced vibration elimination and stability margin extension of the rotor/seal system using the IDVA is proposed in this paper. The rotor/seal system dynamic model is established, and the six configurations of the IDVA are added, respectively, in the system model. The instability threshold speed of the system is obtained by applying the Routh–Hurwitz stability criterion. The QPSO algorithm is utilized to obtain the optimal IDVA parameters. The numerical method is applied to investigate the nonlinear dynamic responses and stability of the rotor/seal system without and with the IDVA. The results are compared with the previous work. The conclusions are drawn as follows.

(1) The IDVA can eliminate the fluid-induced instability vibration and improve the instability threshold speed of the rotor/seal system.

(2) Comparing with the traditional DVA, the effect of the IDVA on the instability vibration elimination and stability improvement is better, but the range of increase in the instability threshold speed is decreased as the damping ratio ζ_a changes.

Data Availability

The data used to support the findings of this study are included within the article.

Conflicts of Interest

The authors declare that there are no conflicts of interest regarding the publication of this paper.

Acknowledgments

The authors would like to gratefully acknowledge the National Natural Science Foundation of China (grant no. U1708257) and the Fundamental Research Funds for Central Universities (no. N180313009) for the financial support for this study.

References

[1] D. E. Bently and A. Muszynska, *Rotordynamics*, CRC Press, Taylor & Francis Group, Boca Raton, USA, 2005.

[2] D. Childs, D. Elrod, and K. Hale, "Annular honeycomb seals: test results for leakage and rotordynamic coefficients; comparisons to labyrinth and smooth configurations," *Journal of Tribology*, vol. 111, no. 2, pp. 293–301, 1989.

[3] P. Varney and I. Green, "Steady-state response of a flexibly mounted stator mechanical face seal subject to dynamic forcing of a flexible rotor," *Journal of Tribology*, vol. 139, no. 6, Article ID 062201, 2017.

[4] M. Arghir, N. Manh-Hung, D. Tonon, and J. Dehouve, "Analytic modeling of floating ring annular seals," *Journal of Engineering for Gas Turbines and Power-Transactions of the ASME*, vol. 134, no. 5, Article ID 052507, 2012.

[5] D. Sun, S. Wang, and Y. Ai, "Theoretical and experimental research on the performance of anti-swirl flow for the static and dynamic characteristics of seals," *Journal of Mechanical Engineering*, vol. 52, no. 3, pp. 101–109, 2016.

[6] H. Zhang, Q. Zheng, G. Yue, and J. Gao, "Numerical analysis of flows and aerodynamic forces in honeycomb and labyrinth seals," *Proceedings of the Institution of Mechanical Engineers, Part C: Journal of Mechanical Engineering Science*, vol. 227, no. 9, pp. 1965–1979, 2013.

[7] H. Zhang, X. Jia, X. Pan, B. Jiang, and Q. Zheng, "Interaction between rotor and annular seals: interlaced and straight-through labyrinth seals," *Journal of Propulsion and Power*, vol. 32, no. 6, pp. 1483–1493, 2016.

[8] X. Jia, H. Zhang, Q. Zheng, S. Fan, and Z. Tian, "Investigation on rotor-labyrinth seal system with variable rotating speed," *International Journal of Turbo & Jet-Engines*, vol. 36, no. 1, pp. 19–29, 2019.

[9] E. Zhang, Y. Jiao, and Z. Chen, "Dynamic behavior analysis of a rotor system based on a nonlinear labyrinth-seal forces model," *Journal of Computational and Nonlinear Dynamics*, vol. 13, no. 10, Article ID 101002, 2018.

[10] H.-L. Hu and L.-D. He, "Online control of critical speed vibrations of a single-span rotor by a rotor dynamic vibration absorber at different installation positions," *Journal of Mechanical Science and Technology*, vol. 31, no. 5, pp. 2075–2081, 2017.

[11] H. Heidari and B. Monjezi, "Vibration control of imbalanced Jeffcott rotor by virtual passive dynamic absorber with optimal parameter values," *Proceedings of the Institution of Mechanical Engineers, Part C: Journal of Mechanical Engineering Science*, vol. 232, no. 23, pp. 4278–4288, 2018.

[12] H. Yao, Z. Chen, and B. Wen, "Dynamic vibration absorber with negative stiffness for rotor system," *Shock and Vibration*, vol. 2016, Article ID 5231704, 13 pages, 2016.

[13] H. Yao, T. Wang, B. Wen, and B. Qiu, "A tunable dynamic vibration absorber for unbalanced rotor system," *Journal of Mechanical Science and Technology*, vol. 32, no. 4, pp. 1519–1528, 2018.

[14] J. Taghipour, M. Dardel, and M. H. Pashaei, "Vibration mitigation of a nonlinear rotor system with linear and nonlinear vibration absorbers," *Mechanism and Machine Theory*, vol. 128, pp. 586–615, 2018.

[15] G. G. Tehrani and M. Dardel, "Mitigation of nonlinear oscillations of a Jeffcott rotor system with an optimized damper and nonlinear energy sink," *International Journal of Non-Linear Mechanics*, vol. 98, pp. 122–136, 2018.

[16] C. Guo, M. A. Al-Shudeifat, A. F. Vakakis, L. A. Bergman, D. M. McFarland, and J. Yan, "Vibration reduction in unbalanced hollow rotor systems with nonlinear energy sinks," *Nonlinear Dynamics*, vol. 79, no. 1, pp. 527–538, 2015.

[17] S. Bab, S. E. Khadem, M. Shahgholi, and A. Abbasi, "Vibration attenuation of a continuous rotor-blisk-journal bearing system employing smooth nonlinear energy sinks," *Mechanical Systems and Signal Processing*, vol. 84, pp. 128–157, 2017.

[18] C. Shi, S. W. Shaw, and R. G. Parker, "Vibration reduction in a tilting rotor using centrifugal pendulum vibration absorbers," *Journal of Sound and Vibration*, vol. 385, pp. 55–68, 2016.

[19] K. Nishimura, T. Ikeda, and Y. Harata, "Localization phenomena in torsional rotating shaft systems with multiple centrifugal pendulum vibration absorbers," *Nonlinear Dynamics*, vol. 83, no. 3, pp. 1705–1726, 2016.

[20] Y. Hu, M. Z. Q. Chen, and Y. Sun, "Comfort-oriented vehicle suspension design with skyhook inerter configuration," *Journal of Sound and Vibration*, vol. 405, pp. 34–47, 2017.

[21] Y. Hu and M. Z. Q. Chen, "Performance evaluation for inerter-based dynamic vibration absorbers," *International Journal of Mechanical Sciences*, vol. 99, pp. 297–307, 2015.

[22] E. Barredo, A. Blanco, J. Colín et al., "Closed-form solutions for the optimal design of inerter-based dynamic vibration absorbers," *International Journal of Mechanical Sciences*, vol. 144, pp. 41–53, 2018.

[23] X. Wang, X. Liu, Y. Shan, Y. Shen, and T. He, "Analysis and optimization of the novel inerter-based dynamic vibration absorbers," *IEEE Access*, vol. 6, pp. 33169–33182, 2018.

[24] M. Lazarek, P. Brzeski, and P. Perlikowski, "Design and identification of parameters of tuned mass damper with inerter which enables changes of inertance," *Mechanism and Machine Theory*, vol. 119, pp. 161–173, 2018.

[25] X. Shi and S. Zhu, "Dynamic characteristics of stay cables with inerter dampers," *Journal of Sound and Vibration*, vol. 423, pp. 287–305, 2018.

[26] J. Luo, J. Z. Jiang, and J. H. G. Macdonald, "Cable vibration suppression with Inerter-Based absorbers," *Journal of Engineering Mechanics*, vol. 145, no. 2, Article ID 04018134, 2019.

[27] Y. Hu, J. Wang, M. Z. Q. Chen, Z. Li, and Y. Sun, "Load mitigation for a barge-type floating offshore wind turbine via inerter-based passive structural control," *Engineering Structures*, vol. 177, pp. 198–209, 2018.

[28] A. Giaralis and F. Petrini, "Wind-induced vibration mitigation in tall buildings using the tuned mass-damper-inerter," *Journal of Structural Engineering*, vol. 143, no. 9, Article ID 04017127, 2017.

[29] Q. Xu, J. Niu, H. Yao, L. Zhao, and B. Wen, "Fluid-induced vibration elimination of a rotor/seal system with the dynamic vibration absorber," *Shock and Vibration*, vol. 2018, Article ID 1738941, 15 pages, 2018.

[30] Q. Xu, J. Niu, H. Yao, L. Zhao, and B. Wen, "Nonlinear dynamic behavior and stability of a rotor/seal system with the dynamic vibration absorber," *Advances in Mechanical Engineering*, vol. 11, no. 1, Article ID 1687814018819578, 2019.

[31] J. Hua, S. Swaddiwudhipong, Z. S. Liu, and Q. Y. Xu, "Numerical analysis of nonlinear rotor—seal system," *Journal of Sound and Vibration*, vol. 283, no. 3–5, pp. 525–542, 2005.

[32] C.-C. Fan and M.-C. Pan, "Active elimination of oil and dry whips in a rotating machine with an electromagnetic actuator," *International Journal of Mechanical Sciences*, vol. 53, no. 2, pp. 126–134, 2011.

[33] Y. Huang, Z. Tian, R. Chen, and H. Cao, "A simpler method to calculate instability threshold speed of hydrodynamic journal bearings," *Mechanism and Machine Theory*, vol. 108, pp. 209–216, 2017.

[34] W. Kim, J. Y. Lee, and J. Chung, "Dynamic analysis for a planetary gear with time-varying pressure angles and contact ratios," *Journal of Sound and Vibration*, vol. 331, no. 4, pp. 883–901, 2012.

[35] H. Ma, H. Li, H. Niu, R. Song, and B. Wen, "Numerical and experimental analysis of the first-and second-mode instability in a rotor-bearing system," *Archive of Applied Mechanics*, vol. 84, no. 4, pp. 519–541, 2014.